The 8th European Congress on Computational Methods in Applied Sciences and Engineering
ECCOMAS Congress 2022
5 – 9 June 2022, Oslo, Norway

TWO CONTINUOUS DUAL STRATEGIES TO SOLVE THE KINEMATICAL AND EQUILIBRIUM PROBLEM FOR MASONRY-LIKE STRUCTURES

ANDREA MONTANINO[1], CARLO OLIVIERI[2], DANIELA DE GREGORIO[1], AND ANTONINO IANNUZZO[3]

[1] Dept. of Structures for Engineering and Architecture, University of Naples Federico II,
Via Claudio 21, 80125, Naples (ITALY) -
{andrea.montanino,daniela.degregorio}@unina.it

[2] Dept. of Civil Engineering, University of Salerno,
Via Giovanni Paolo II, 84084, Fisciano (ITALY) - colivieri@unisa.it

[3] ETH Zurich, Inst. of Technology in Architecture, Stefano-Franscini-Platz 1, CH-8093
Zurich (SWITZERLAND) - iannuzzo@arch.ethz.ch

Key words: no-tension materials, singular stresses, singular and smeared fractures, settlements, constrained optimisation problems.

Abstract. Nowadays, there is a raising interest in the development of fast and robust tools to detect the consequences of settlements or loading changes in unreinforced masonry buildings, since they constitute a large part of world architectural heritage. Current tools, based on Finite Element Method or on Discrete Element Method are computationally cumbersome, from one side due to difficulties in dealing with unilateral materials, and on the other side, due to the need of formulating the problem as an explicit dynamics problem. The methods proposed here are based on the minimization problem of two different functionals, the Total Potential Energy, and the Total Complementary Energy, which allow to detect the stress and strain distribution developed under given load and given boundary settlements, through a minimization problem, which require a significantly lower computational cost and no material parameters, especially when rigidity assumption of the material is done. After illustrating the main characteristics of the two methods, they are applied to a case study, and the results are suitably described and discussed.

1 INTRODUCTION

Most buildings of historical and cultural interest, especially in Europe, are made of unreinforced masonry (URM). Though they represent the most ancient and resilient construction technology, their mechanical behaviour is currently undergoing an in-depth scientific investigation. The purpose is to develop techniques to predict their behaviour under different actions and preserve them. URM shows a complex mechanical response: it has good compressive strength but little tensile strength. These properties make masonry structures very ductile for variations in the boundary conditions, such as settlements or distortions. Because of the material behaviour, these actions result in cracks, often intimidating technicians who

approach restoration projects through over-conservative, sometimes unnecessary solutions.

The most applied analysis approach is the finite element method (FEM) [1, 2, 3], which can address complex geometrical problems and model a large variety of material constitutive relations. Despite their widespread use, much research has shown that the standard FEM approach fails to capture the fundamental aspects of unilateral structures. In recent works, FEM has been used to evaluate unilateral assemblies by modelling each block as a distinct element [4], however, succeeding only in providing yes-no answers. Thus, other optimisation processes, such as gradient-based optimisation formulations, cannot be incorporated.

In last decades, another widely used method for 3D finite displacement analysis is the discrete element modelling (DEM) [5, 6, 7, 8, 9]. It can analyse block-based structures, model various loading conditions, consider any kinematic and dynamic data. A DEM model requires three features: i) detecting contacts; ii) allow detachment; and, iii) allow new contact formation. The behaviour is modelled through explicit dynamics, where the interaction among blocks is assumed unilateral. Nonetheless, both FE and DEM require detailed material description, and a careful modelling of mechanical and numerical parameters. Moreover, also because of these aspects, they are computationally demanding, making sometimes impossible to fully explore several mechanical scenarios.

A widely accepted approach for masonry structures is represented by Limit Analysis (LA), in which the number of mechanical parameters is drastically reduced (e.g. in many cases only the friction angle or compressive strength is required [10, 11]). Particularly, it is always applied referring to its Upper Bound and Lower Bound formulations. Focusing on classical limit analysis approaches, i.e., based on the model proposed in the 1960s by Heyman [12], it is possible to describe the material without using any mechanical parameters, i.e., normal, rigid and non reacting in tension (NRNT) [13]. Based on this model, recently, several models based on the lower bound approach have been developed to deal with complex 3D problems. Indeed, we find models based on the Thrust Line analysis [14, 15, 16, 17, 18, 19], their extension to 3D, namely, the Linear Arch Static Analysis (LASA) [20, 21], Thrust Network Analysis (TNA) [22, 23, 24], and Membrane Equilibrium Analysis (MEA) [25, 26, 27, 28, 29, 30, 31]. A DEM-like model has been recently developed to analyse in a fast way 2D block structures based on the upper bound approach using minimum energy criteria, namely, the Piecewise Rigid Displacement (PRD) [32, 33, 34, 35].

This contribution aims at illustrating and comparing two methodologies that can solve the boundary value problem for URM structures, adopting a displacement or an equilibrium approach [36]. Both methods have the advantage of being mesh-independent, considering the analysed structure as a continuous body. The first method, the Continuous Displacement for Fracture (CDF) [37], is based on a FE mesh discretisation of the structural domain, in which the displacements are assumed as continuous, and for which the solution is found by minimising the Total Potential Energy. On the other hand, the Continuous Airy-based for Stress-Singularities (CASS) [38], again considering a FE discretisation of the domain, looks for the stress solution by solving a constrained optimisation problem through minimisation of the Total Complementary Energy. Thanks to this approach, it is possible to identify fractures or stress singularities, which appear as smeared on narrow bands.

In order to show the quality of the solutions found with both methods and to identify their substantial differences, they will be applied to two case studies known from the literature.

2 BOUNDARY VALUE PROBLEM FOR A NORMAL, RIGID NO-TENSION MATERIAL

In this paragraph the boundary value problem (BVP) for a continuum Ω composed of normal rigid no-tension (NRNT) material is introduced. In particular, the BVP reads:

"Find a stress $\boldsymbol{T}$, a strain $\boldsymbol{E}$ and a displacement $\boldsymbol{u}$ fields having Ω as support, such that the following three conditions hold:

$$\mathbf{E} = \frac{1}{2}(\nabla\mathbf{u} + \nabla\mathbf{u}^{\mathrm{T}}) \ , \ \mathbf{E} \in \mathrm{Sym}^{+} \ , \ \mathbf{u} = \bar{\mathbf{u}} \ \mathrm{on} \ \partial\Omega^{\mathrm{D}} \ , \tag{1}$$

$$\mathrm{div}\mathbf{T} + \mathbf{b} = \mathbf{0} \ , \ \mathbf{T} \in \mathrm{Sym}^{-} \ , \ \mathbf{T}\mathbf{n} = \bar{\mathbf{p}} \ \mathrm{on} \ \partial\Omega^{\mathrm{N}} \tag{2}$$

$$\mathbf{T} \cdot \mathbf{E} = 0 \tag{3}$$

where $\bar{\mathbf{p}}$, $\mathbf{b}$ are the surface and body loads applied on the loaded part of the domain boundary $\partial\Omega^{\mathrm{N}}$, and on the domain interior Ω, respectively; $\bar{\mathbf{u}}$ is the boundary displacement field (i.e. settlements) on the constrained part of the domain boundary $\partial\Omega^{D}$. Figure 1 shows a graphical representation of the semidefinite positive and negative cones Sym^{+} and Sym^{-}, where the stresses and the strains of an NRNT continuum live.

The solution of the BVP can be obtained with different strategies. In the present paper two variational criteria are used to find two dual solutions in terms of stress and displacements. Specifically, the two criteria are based on the minimum of the total potential and complementary energy. With the former the solution is sought in the space $\mathcal{K}$ of the kinematically admissible displacements while the latter finds the solution in the space $\mathcal{H}$ of the equilibrated admissible stresses. It is worth noting that minimum of the total potential energy selects the admissible displacement that also satisfies the equilibrium relations (2); conversely, the minimum of the total complementary potential energy provides a minimiser $\mathbf{T}^{\circ}$ that satisfies the kinematic compatibilities (1). In the next subsections, these two variational criteria are briefly introduced.

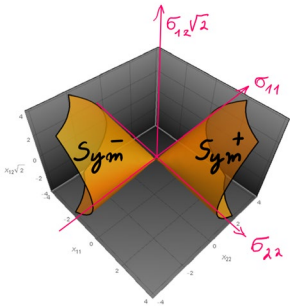

Figure 1: Graphical representation of the positive and negative semidefinite cones.

2.1 Minimum of the total complementary energy

The BVP solution for a body Ω composed of NRNT material and subject to the load $\{\bar{\mathbf{p}}, \mathbf{b}\}$ and to the distortion data $\bar{\mathbf{u}}$, such that $\mathbf{u} \in \mathcal{K}$, $\mathbf{T} \in \mathcal{H}$ and $\mathbf{T} \cdot \mathbf{E} = 0$, can be also obtained as the minimizer of the complementary energy

$$\mathcal{E}_{\mathrm{c}}(\mathbf{T}) = -\int_{\partial\,\partial\Omega^{\mathrm{D}}} \mathbf{T}\mathbf{n} \cdot \bar{\mathbf{u}} \mathrm{d}s. \tag{4}$$

Where $\mathcal{E}_c(\mathbf{T})$ is a functional defined over $\mathcal{H}$. The minimiser $\mathbf{T}^\circ$ of $\mathcal{E}_c(\mathbf{T})$

$$\mathcal{E}_c(\mathbf{T}^\circ) = \min_{\mathbf{T}\in\mathcal{H}} \mathcal{E}_c(\mathbf{T}) \,. \tag{5}$$

represents the solution of the BVP, if it exists.

2.1 Minimum of the total potential energy

A BVP solution for a body Ω composed of NRNT material and subject to the load data $\{\overline{\boldsymbol{p}}, \boldsymbol{b}\}$ and to the distortion data $\overline{\boldsymbol{u}}$, such that $\boldsymbol{u} \in \mathcal{K}$, $\boldsymbol{T} \in \mathcal{H}$ and $\boldsymbol{T} \cdot \boldsymbol{E} = 0$, can be also obtained through a dual criterion, i.e. the minimum of the total potential energy

$$\mathcal{E}_p(\mathbf{u}) = -\int_{\partial\partial\Omega^N} \overline{\mathbf{p}} \cdot \mathbf{u} \mathrm{ds} - \int_\Omega \mathbf{b} \cdot \mathbf{u} \mathrm{da} \,. \tag{6}$$

$\mathcal{E}(\mathbf{u})$ is a functional of the displacement $\mathbf{u}$ and having $\mathcal{K}$ as support. Among the infinite $\mathbf{u} \in \mathcal{K}$, its minimiser $\mathbf{u}^\circ$, if any, corresponds to the solution of the BVP:

$$\mathcal{E}_p(\mathbf{u}^\circ) = \min_{\mathbf{u}\in\mathcal{K}} \mathcal{E}(\mathbf{u}). \tag{7}$$

3 NUMERICAL FORMULATION

Here we briefly recall the fundamentals of the numerical methods adopted to discretise and solve the BVP for masonry-like structures made of NRNT material and subjected to given loads and settlements. Two discretisation techniques are adopted. It is worth noting that even though the functional spaces over which they are defined are composed of continuous functionals, the use of a rigid material model allows for modelling concentrated stress and strains, as demonstrated in Kao [39].

In particular, the minimum of the complementary energy is solved using the Continuous Airy-based Stress for Singularities (CASS) method and of the displacement field is found through the Continuous Displacement for Fractures (CDF) method.

3.1 Continuous Airy-based Stress for Singularities

The Continuous Airy-based Stress for Singularities is a numerical method based on the Airy stress formulation of the equilibrium problem, where the stress can be expressed in terms of the curvature of a stress function F, as

$$\mathrm{T_{xx}} = \frac{\partial^2 \mathrm{F}}{\partial \mathrm{y}^2} \quad , \quad \mathrm{T_{yy}} = \frac{\partial^2 \mathrm{F}}{\partial \mathrm{x}^2} \quad , \quad \mathrm{T_{xy}} = -\frac{\partial^2 \mathrm{F}}{\partial \mathrm{x}\,\partial \mathrm{y}} \tag{8}$$

Therefore, the Total Complementary energy is minimized in the set $\mathcal{H}_F$ of the admissible Airy stress functions., which requires

$$\mathrm{tr}\big(\mathbf{H}(\mathrm{F})\big) < 0 \quad , \qquad \det\big(\mathbf{H}(\mathrm{F})\big) > 0 \quad , \tag{9}$$

being $\mathbf{H}(\mathrm{F})$ the Hessian of the Airy stress function. Condition (9) implies the convexity of the Airy stress potential on Ω.

The domain is divided in a finite number of rectangular plate-type finite elements, with dimensions L and H, as shown in Figure 2

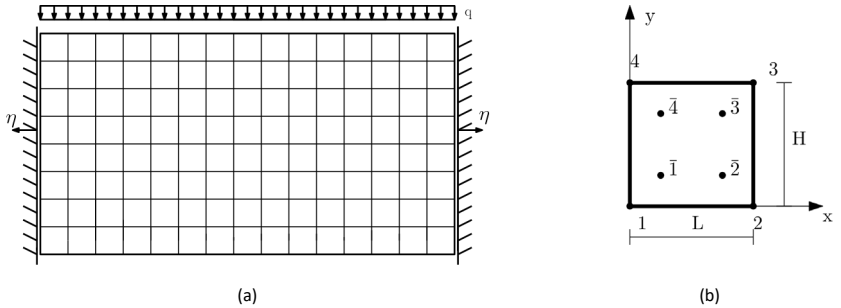

Figure 2: (a) CASS FE discretization; (b) element characteristics.

Three degrees of freedom are associated to each element node, that are the values of the Airy stress potential and its derivatives in the x- and y-directions. This choices assures the continuity of the stress function across the element boundary, and the continuity of the derivative in the direction tangent to the boundary, that is, continuity of the tractions along the elemnt boundaries.

The convenience of the choice of the Airy stress formulation is based on the fact that the equilibrium is implicitly satisfied. To comply with the constraint (9), the Hessian $\mathbf{H}(\mathrm{F})$ is computed on four internal nodes of each elements (see Figure 2b), and can be reformulated in terms of the degrees of freedom $\hat{\mathbf{F}}$ at the mesh nodes, as

$$\hat{\mathbf{T}}_{\mathbf{xx}} = \mathbf{K}_{\mathbf{xx}}\hat{\mathbf{F}} \quad , \quad \hat{\mathbf{T}}_{\mathrm{yy}} = \mathbf{K}_{\mathrm{yy}}\hat{\mathbf{F}} \quad , \quad \hat{\mathbf{T}}_{\mathrm{xy}} = \mathbf{K}_{\mathrm{xy}}\hat{\mathbf{F}} \quad , \tag{10}$$

being $\mathbf{K}_{\mathbf{xx}}$, $\mathbf{K}_{\mathrm{yy}}$, and $\mathbf{K}_{\mathrm{xy}}$ coefficient matrices depending on the shape of the element. Condition (9), rewritten in terms of Equation (10), define a set of conic inequality constraints, in the form

$$\mathbf{K}_{\Omega}\hat{\mathbf{F}} \leq \mathbf{0} \ , \tag{11}$$

The stress boundary conditions are imposed in terms of the derivatives of the Airy stress potential, in the normal and in the tangential directions, and result in a linear system as

$$\mathbf{K}_{\partial\Omega}\hat{\mathbf{F}} = \mathbf{b}_{\partial\Omega} \quad . \tag{12}$$

Following [40], it can be shown that the boundary values of the Airy stress potential correspond to the contact moment $\mathrm{m}(\mathrm{s})$ of a frame structure having the same shape of $\partial\Omega^{\mathrm{N}}$ under the boundary loads, and that the normal derivative of the Airy stress function $\partial F/\partial n$ corresponds to the internal axial forces $\mathrm{n}(\mathrm{s})$ on the same frame structure.

Finally, the discretised version of the Total Complementary Energy, under the hypotheses of rigidity of the material can be written as

$$\mathcal{E}_{\mathrm{c}}(\hat{\mathbf{F}}) = \mathbf{g}^{\mathrm{T}}\hat{\mathbf{F}} \quad . \tag{13}$$

The discrete problem, therefore, can be rewritten as

$$\mathcal{E}_{\mathrm{c}}(\hat{\mathbf{F}}^{\circ}) = \min_{\hat{\mathbf{F}} \in \mathcal{H}^{\mathrm{N}}_{\mathrm{CASS}}} \mathcal{E}_{\mathrm{c}}(\hat{\mathbf{F}}) \quad , \tag{14}$$

where

$$\mathcal{H}^{\mathrm{N}}_{\mathrm{CASS}} = \{\hat{\mathbf{F}} \in \mathbb{R}^{3\mathrm{N}} \ / \ \mathbf{K}_{\Omega}\hat{\mathbf{F}} \leq \mathbf{0} \, , \qquad \mathbf{K}_{\partial\Omega}\hat{\mathbf{F}} = \mathbf{b}_{\partial\Omega} \} \tag{15}$$

Problem (15) is a minimisation problem with linear objective function, linear equality constraints and conic inequality constraints, easily solved by robust and well-established numerical tools.

3.2 Continuous Displacement for Fractures

This Section illustrates the CDF method. The solution of the minimum problem (X) is approximated in the set of continuous, piecewise polynomial displacement fields generated by a quadrangular FE mesh made up of nine-node Lagrangian elements. The choice of the element's typology used to approximate the displacement field is not entirely free (for more details the reader is referred to [ref, CAS]). The displacements are continuous on the domain as in standard FE approaches. Therefore, the strain is regular and does not show any jump.

Let $(\Omega_i)_{i\in\{1,2,..,M\}}$ be the partition of the domain into nine-node Lagrangian elements. The integer number N denotes the total number of nodes generated by the partition nad the selected shape functions. The displacement field $\mathbf{u}$ can be expressed as:

$$\mathbf{u} = \mathbf{u}(\mathbf{U}) , \tag{16}$$

with the vector $\mathbf{U} = (U_1, V_1, .., U_i, V_i, .., U_N, V_N)$ collecting all scalar parameters (U_i, V_i) expressing the displacement of the node i.

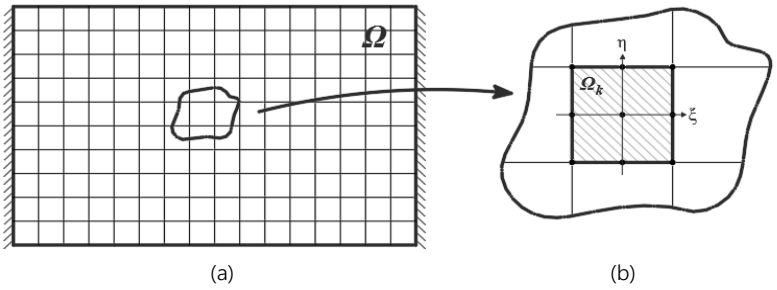

Figure 3: (a) FE discretisation of the domain Ω; (b) subdomain Ω_k and a second order 9-noded finite element.

The latent strain can thus be expressed as function of the nodal displacements:

$$\mathbf{E}_k = \mathbf{E}|_{\Omega_k} = \mathrm{Sym}\nabla\mathbf{u}_k \ . \tag{17}$$

with

$$\mathbf{u}_k = \mathbf{u}|_{\Omega_k} , \tag{18}$$

being the displacement field on the finite element Ω_k. The condition on the latent strain $\mathbf{E}$ as belonging to the semidefinite positive cones, can be enforced on the internal points $(\tilde{x}, \tilde{y})$ of each element as:

$$\mathbf{E}_k(\tilde{x}, \tilde{y}) \in Sym^+ . \tag{19}$$

This condition is equivalent to the two following relations:

$$\mathrm{tr}\mathbf{E} \geq 0 \ , \qquad \det\mathbf{E} \geq 0 \ . \tag{20}$$

Conditions (19) define the convex set of the semidefinite positive symmetric tensors.

From a numerical standpoint, the previous condition can be either enforced directly by a second-order rotated cone, or can be linearised, as described in [paper CAS]. The linearisation scheme can be expressed in a matrix form as:

$$\mathbf{A}_k(\tilde{x}, \tilde{y})\, \mathbf{U}_k \geq \mathbf{0} , \tag{21}$$

with the matrix $\mathbf{A}_k(\tilde{x}, \tilde{y})$ collecting the coefficients of the hyperplanes tangent to the cone on the nodes of the element k, and the vector $\mathbf{U}_\mathrm{k}$ collecting the nodal displacements of the element k. These restrictions can be written for each element and, then, collected on the whole domain as:

$$\mathbf{A}\,\mathbf{U} \geq \mathbf{0} \ . \tag{22}$$

The non-homogeneous boundary conditions are summarised in a matrix form as:

$$\mathbf{B}\mathbf{U} = \overline{\mathbf{U}} \ . \tag{23}$$

where $\mathbf{B}$ is the extractor operator that selects the nodes on the constrained boundary, while $\overline{\mathbf{U}}$ collects the prescribed settlements. Inequalities (22) and boundary conditions (23) define the set of admissible displacements:

$$\mathbb{K}^{\mathrm{N}}_{\mathrm{CDF}} = \left\{\mathbf{U} \in \mathbb{R}^{2\mathrm{N}} \,/\, \mathbf{A}\,\mathbf{U} \geq \mathbf{0}\,, \qquad \mathbf{B}\mathbf{U} = \overline{\mathbf{U}}\right\} \tag{24}$$

that discretises the infinite dimensional set $\mathcal{K}$. With this discretisation, the minimum problem (24) can be approximated through the following finite dimensional one:

$$\wp(\mathbf{U}^{\mathrm{o}}_{\mathrm{CDF}}) = \min_{\hat{\mathbf{U}} \in \mathbb{K}^{\mathrm{N}}_{\mathrm{CDF}}} \wp(\mathbf{U}) \tag{25}$$

With the above approximation the structural problem is solved finding the vector of nodal displacements $\mathbf{U}^{\mathrm{o}}_{\mathrm{CDF}}$ that minimise the linear function $\wp$ expressing the total potential energy in the set $\mathbb{K}^{\mathrm{N}}_{\mathrm{CDF}}$. Problem (25) is a linear programming problem. Once the problem is solved, the deformed configuration of the structure can be constructed from $\mathbf{U}^{\mathrm{o}}_{\mathrm{CDF}}$, and the strain can be obtained differentiating the displacement fields as combination of nodal displacements and shape functions.

4 APPLICATION

In this Section, an application of the CDF method for the recovery of the deformation field, and of the CASS method for the stress solution, are presented. In particular, a masonry façade, with geometry shown in Figure 4, is studied under the effect of given vertical loads, and the settlement of the central pile.

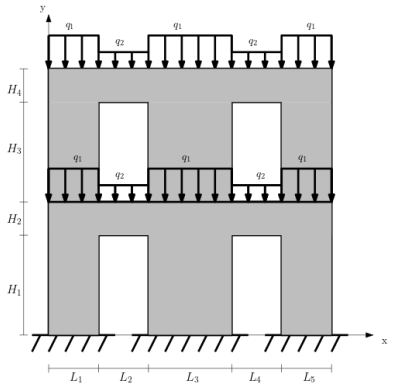

Figure 4: Geometry and loading conditions for the problem of the masonry façade under settlement.

The dimensions are $\mathrm{L}_1 = \mathrm{L}_2 = \mathrm{L}_4 = \mathrm{L}_5 = 1.5$ m, $\mathrm{L}_3 = 2.5$ m, $\mathrm{H}_1 = \mathrm{H}_3 = 3$ m, $\mathrm{H}_2 = \mathrm{H}_4 =$

1 m. The applied loads are $q_1 = \alpha(H_1 + H_2)$, and $\alpha = q_0 H_2$, with $\alpha = 1$ kN/m^2. The settlement of the central pile is $\eta = 10^{-3}$m downwards.

4.1 CASS analysis

As shown in Section 3.1, the solution of this problems requires the definition of the contact moment $m(s)$ and of the axial force $n(s)$ on a beam structure having the same shape of the Neumann boundary $\partial\Omega_N$. In particular, for the present case, the contact moment is parabolic on the top side of the domain, with curvatures proportional to the intensity of the applied distributed loads. We remark that the contact moment, and therefore, the value of the Airy stress potential, is C^1-continuous at the jumps of the values of the applied loads. On the vertical sides, $m(s)$ is constant, with a jump in correspondence of the load applied at the first floor. A representation of such boundary condition is shown in Figure 5

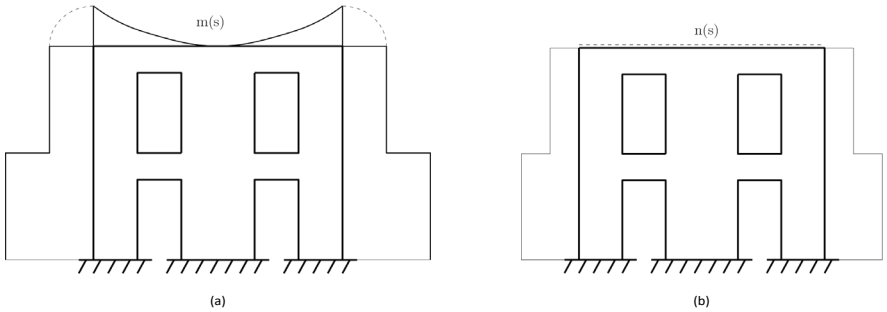

Figure 5: Boundary conditions for the problem of the masonry façade in terms of the internal actions $m(s)$ and $n(s)$

On the other hand, the contact axial force $n(s)$ vanishes on the top side, and is constant on the lateral side, again presenting a jump in correspondence of the load at the intermediate floor. For each of the internal openings, the Airy stress function belongs to a plane, and consequently the slope of the Airy stress potential is the same for all nodes belonging to that opening.

The objective function can be computed as

$$\mathcal{E}_c = -\int_{P_1}^{P_2} T_{xy}\eta \, dx = \int_{P_1}^{P_2} F_{,xy}\, \eta \, dx = \eta\left[F_{,y}(P_2) - F_{,y}(P_1)\right] \tag{26}$$

By solution of the discrete problem (14) under the boundary conditions depicted in Figure 5, and the stress admissibility constraints, we get the solution shown in Figure 6a in terms of the Airy stress function, and in Figure 6b in terms of the minimum principal stress.

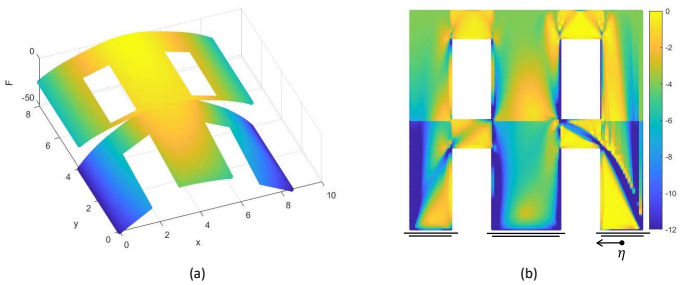

Figure 6: (a) Airy stress potential and (b) minimum principal stress distribution for the problem of the masonry façade.

4.2 CDF analysis

This method describes the minimum of the total potential energy as a second order convex programming, or as here implemented, as a linear programming problem through a outer linear envelope of the semidefinite convex cones, to which the strain tensor has to belong. It is worth noting that this material restrictions are directly enforced as constraints of the problem.

The external loads here considered are the distributed loads applied on the two story-levels, and they are directly considered in the objective function, which reads:

$$E_p = -\int_\gamma \mathbf{q} \cdot \mathbf{u}\, dx = -\mathbf{F}\,\mathbf{U}_q = -\mathbf{F}\,\mathbf{B}_q\mathbf{U} \tag{27}$$

where the external distributed loads $\mathbf{q}$ are lumped to the relevant nodes $\mathbf{U}_q$ and collected into the vector $\mathbf{F}$. $\mathbf{B}_q$ is the linear operator that extracts the loaded nodes $\mathbf{U}_q$ from the vector $\mathbf{U}$. It is worth noting that the boundary conditions are enforces as:

$$\mathbf{u} \cdot \mathbf{n} \geq \mathbf{0}\,, \mathbf{u} \cdot \mathbf{t} = \boldsymbol{\delta} \tag{28}$$

where $\mathbf{n}$ is the normal unit vector to the boundary pointing inside the domain, and t is the tangential unit vector. Note that $\boldsymbol{\delta}$ is 0 everywhere except for the base of the right panel, where is constant and equal to the external settlement. The result of the CDF analysis returns the solution depicted in Figure 7.

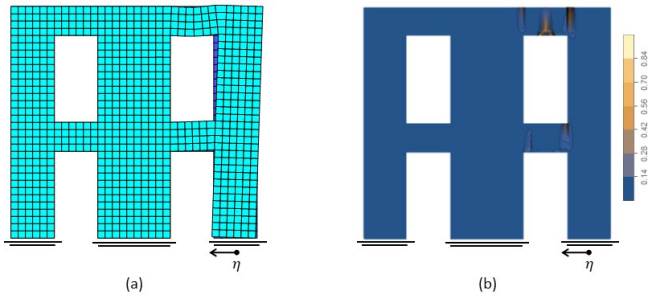

Figure 7: Displacement of the masonry façade subjected to the inward horizontal settlement and contour plot of the strain tensor norm showing the region where cracks appear (b).

4.3 Discussion

The complementarity of che CASS and CDF method are here analysed I terms of the proposed example, in particular we aim at highlighting the reconcilability of the stresses obtained through the minimization fo the Total Complementary Energy with the deformation retrieved through the minimisation of the Total Potential Energy, in the sense of Equation (3). In fact, where unstressed zone are shown, fractures are expected, while, in presence of biaxial compressive stress zones, fracture is expected not to occur.

From Figure 7b, in particular, we notice some vertical, singular deformations above the right window, which correspond to unloaded zones in Figure 6b; the same occurs above the right portal, where the deformed configurations show the formation of a compressed panel, precisely captured by the stress distribution got through the CASS method.

5 CONCLUSIONS

In this paper we developed two complementary strategies to detect the behaviour of masonry structures, the first based on the analysis of stresses, the latter of the deformation. Both strategies descend from the Heyman's principle of Limit Analysis applied to masonry material. In particular, the CASS method is based on the minimization of the Total Complementary Energy, reformulated in terms of an Airy stress potential. On the other hand, the CDF method investigates the material deformation through the minimization of a Total Potential Energy. Both methods work in a continuous framework, that is however able to capture stress and strain singularities, making both methods absolutely mesh independent.

The results described in the last section show the validity of the methods in terms of accuracy and robustness, and a reciprocal benchmarking ability, showing compatible and reconcilable stress and strain fields, in accordance with the requirements of the investigated boundary value problem.

REFERENCES

[1] Lourenço, P.B., and Rots J.G., "Multisurface interface model for analysis of masonry," *J Eng Mech,* no. 123(7), pp. 660-8, 1997.

[2] Reccia, E., Milani, G., Cecchi, A., Tralli, A., "Full 3D homogenization approach to investigate the behavior of masonry arch bridges: The Venice trans-lagoon railway bridge," *Constr Build Mater,* no. 66, pp. 567-586, 2014.

[3] Liberatore, D., Addessi, D., Sangirardi, M., "A force-based macroelement for the nonlinear dynamic analysis of masonry buildings," in *AIMETA 2017 XXIII conference. The Italian Association of Theoretical and Applied Mechanics*, Salerno, Italy, 2017.

[4] Papadopoulos, K. A., "Seismic stability assessment of an ancient dry stone defensive wall," *Bulletin of Earthquake Engineering,* no. 19(1), pp. 463-482, 2021.

[5] Lemos, J.V., "Discrete element modeling of masonry structures," *Int J Archit Herit,* no. 1(2), p. 190–213, 2007.

[6] Tóth, A., Orbán, Z., Bagi, K., "Discrete element analysis of a stone masonry arch," *MRC,* no. 36(4), p. 469–480, 2009.

[7] Forgács, T., Sarhosis, V., Bagi, K., "Minimum thickness of semi-circular skewed masonry arches," *Eng Struct,* no. 140, p. 317–336, 2017.

[8] McInerney, J., and DeJong, M.J., "Discrete element modeling of groin vault displacement capacity," *Int J Archit Herit,* no. 9(8), p. 1037–1049, 2015.

[9] Gobbin, F., de Felice, G., Lemos, J.V., "Numerical procedures for the analysis of collapse mechanisms of masonry structures using discrete element modelling," *Eng. Struc.,* no. 246, p. 113047, 2021.

[10] Portioli F., Casapulla, C., Cascini, L., "n efficient solution procedure for crushing failure in 3D limit analysis of masonry block structures with non-associative frictional joints," *IJSS,* vol. 69, pp. 252-266, 2015.

[11] D'Ayala D., and Casapulla C., "Limit state analysis of hemispherical domes with finite friction," *Historical constructions, possibilities of numerical and experimental*

techniques, pp. 617-626, 2001.

[12] Heyman, J., "The stone skeleton," *Int Journal of Solids Structures,* no. 2(2), p. 249–279, 1966.

[13] Angelillo, M., "Practical applications of unilateral models to Masonry Equilibrium," in *Angelillo M, editor. Mechanics of Masonry Structures*, Vienna, Springer, 2014.

[14] Cusano, C., Montanino, A., Olivieri, C., Paris, V., Cennamo, C., "Graphical and analytical quantitative comparison in the domes assessment: The case of san francesco di paola," *Appli Sci,* no. 11(8), p. 3622, 2021.

[15] Como, M., Statics of historic masonry constructions, Berlin: Springer, 2013.

[16] Huerta Fernández S., "Geometry and equilibrium: The gothic theory of structural design," *Struc Eng,* vol. 84, no. 2, pp. 23-28, 2006.

[17] Huerta Fernández S., "Galileo was wrong: the geometrical design of masonry arches," *Nexus Network Journal,* no. 8(2), pp. 25-52, 2006.

[18] Ochsendorf J., Collapse of masonry structures, Doctoral dissertation: University of Cambridge, 2002.

[19] Cusano, C., Angjeliu, G., Montanino, A., Zuccaro, G., Cennamo, C., "Considerations about the static response of masonry domes: A comparison between limit analysis and finite element method," *IJMRI,* vol. 6, no. 4, pp. 502-528, 2021.

[20] Angelillo, M., Olivieri, C., DeJong, M.J., "A new equilibrium solution for masonry spiral stairs," *Eng Struc,* vol. 238, p. 112176, 2021. DOI: 10.1016/j.engstruct.2021.112176.

[21] Olivieri, C., Cennamo, C., Cusano, C., Cutolo, A., Fortunato, A., Mascolo, I., "Masonry Spiral Stairs: A Comparison between Analytical and Numerical Approaches," *Appli Sci,* no. 12(9), p. 4274, 2022.

[22] Block P, Thrust Network Analysis: Exploring Three-dimensional Equilibrium, Massachusetts Institute of TechnologyCambridge, MA, USA: PhD dissertation, 2009 (May).

[23] Block, P., and Ochsendorf, J., "Thrust network analysis: a new methodology for three-dimensional equilibrium," *IASS J.,* vol. 48, no. 3, pp. 167-173, 2007.

[24] Avelino, R. M., Iannuzzo, A., Van Mele, T., Block, P., "Assessing the safety of vaulted masonry structures using thrust network analysis.," *Comp & Struc,* no. 257, p. 106647, 2021.

[25] Angelillo M, Fortunato A, "Equilibrium of masonry vaults," *Novel Approaches in Civil Engineering, M. Fremond, F. Maceri Ed's, Lecture Notes in Applied and Computational Mechanics, Springer, Berlin,* vol. 16, pp. 105-109, 2004.

[26] Angelillo, M., Babilio, E., Fortunato, A., "Singular stress fields for masonry-like vaults," *Continuum Mechanics and Thermodynamics,* vol. 25, pp. 423-441, 2013.

[27] De Chiara, E., Cennamo, C., Gesualdo, A., Montanino, A., Olivieri, C., Fortunato. A., "Automatic generation of statically admissible stress fields in masonry vaults.," *JOMMS,* vol. 14(5), pp. 719-737, 2019.

[28] Gesualdo, A., Brandonisio, G., De Luca, A., Iannuzzo, A., Montanino, A., Olivieri, C., "Limit analysis of cloister vaults: The case study of Palazzo Caracciolo di Avellino.

Journal of Mechanics of Materials and Structures," *JOMMS,* no. 14(5), pp. 739-750, 2019.

[29] Olivieri, C., Fortunato, A., DeJong, M.J., "A new membrane equilibrium solution for masonry railway bridges: The case study of Marsh Lane Bridge," *IJMRI,* no. 6(4), pp. 446-471, 2021.

[30] Montanino, A., Olivieri, C., Zuccaro, G., Angelillo, M., "From stress to shape: equilibrium of cloister and cross vaults," *Appli Sci,* vol. 11, no. 9, 2021, DOI: 10.3390/app11093846.

[31] C. Cusano, A. Montanino, C. Cennao, G. Zuccaro and M. Angelillo, "Geometry and Stability of a Double-shell Dome in Four Building Phases: The Case Study of Santa Maria Alla Sanità in Naples," *Int. Jour. Arch: Her.,* pp. 1-27, 2021.

[32] Iannuzzo, A., "Energy based fracture identification in masonry structures: the case study of the church of "Pietà dei Turchini"," *JOMMS,* vol. 5, no. 14, pp. 683-702, 2019.

[33] Iannuzzo, A., Olivieri, C., Fortunato, A., "Displacement capacity of masonry structures under horizontal actions via PRD method," *JOMMS,* vol. 5, no. 14, pp. 703-718, 2019.

[34] Iannuzzo, A., Angelillo, M., De Chiara, E., De Guglielmo, F., De Serio, F., Ribera, F., Gesualdo, A., "Modelling the cracks produced by settlements in masonry structures," *Meccanica,* vol. 7, no. 53, pp. 1857-1873, 2018.

[35] Iannuzzo, A., Van Mele, T., Block, P., "Piecewise rigid displacement (PRD) method: a limit analysis-based approach to detect mechanisms and internal forces through two dual energy criteria," *Mech. Res. Commun.,* vol. 107, p. 103557, 2020.

[36] Roca, P., Cervera, M., G. Gariup, G., Pelà, L., "Structural Analysis of Masonry Historical Constructions. Classical and Advanced Approaches," *Arch. Computat. Methods Eng.,* no. 17, p. 299–325, 2010.

[37] Iannuzzo, A., Angelillo, M., Block, P., Gesualdo, A., "A continuous energy-based numerical approach to predict fracture mechanisms in masonry structures: CDF method," *Comp and Struc,* no. 257, p. 106645, 2021.

[38] A. Montanino, D. De Gregorio and A. Iannuzzo, "The continuous Airy-based for stress-singularities (CASS) method: an energy-based numerical formulation for unilateral materials," *IJSS,* p. Under review, 2022.

[39] G. Kao, A. Iannuzzo, B. Thomaszewski, S. Coros, T. Van Mele and P. Block, "Coupled Rigid-Block Analysis: Stability-Aware Design of Complex Discrete-Element Assemblies.," *Computer-Aided Design,* vol. 146, p. 103216., 2022.

[40] M. Angelillo , A. Fortunato, A. Montanino and M. Lippiello, "Singular stress fields in masonry structures: Derand was right.," *Meccanica,* vol. 49, no. 5, pp. 1243-1262., 2014.